Evidence for quasi-periodic X-ray dips from an ULX: Implications for the binary motion and the orbital inclination

Dheeraj R. Pasham[1] & Tod E. Strohmayer[2]

ABSTRACT

We report results from long-term X-ray (0.3-8.0 keV) monitoring of the ultraluminous X-ray source NGC 5408 X-1 with the *Swift*/X-Ray Telescope. Our primary results are: (1) the discovery of quasi-periodic dips in the X-ray intensity that recur on average every 243 days, (2) the detection of an energy-dependent (variability amplitude decreases with increasing energy), quasi-sinusoidal X-ray modulation with a period of 112.6±4 days the amplitude of which decreases during the second half of the light curve and (3) energy spectral evidence for an increase in photoelectric absorption during the last continuous segment of the data, possibly due to a change in the ionization state of the circumbinary material. We interpret the X-ray modulations in the context of binary motion in analogy to that seen in high-inclination low-mass X-ray binaries. If correct, this implies that NGC 5408 X-1 is in a binary with an orbital period of 243±23 days in contrast to the 115.5 day quasi-sinusoidal period previously reported. In addition, if the X-ray modulation is caused by vertically structured obscuring material in the accretion disk (similar to the phenomenon of dipping LMXBs), this would imply a high value for the inclination of the orbit. A comparison with estimates from accreting X-ray binaries suggests an inclination $\gtrsim 60°$. We note that, in principle, a precessing accretion disk could also produce the observed X-ray modulations.

Subject headings: Ultraluminous X-ray source ; NGC 5408 X-1 : X-ray dipper : Intermediate-mass black hole (IMBH) candidate: High orbital inclination

1. Introduction & Background

Ultraluminous X-ray sources (ULXs) are bright, point-like, extragalactic sources whose X-ray luminosities have values in the range of a few $\times$ 10^{39} ergs s^{-1} to as high as 10^{41}

[1]Astronomy Department, University of Maryland, College Park, MD 20742; dheeraj@astro.umd.edu

[2]Astrophysics Science Division, NASA's Goddard Space Flight Center, Greenbelt, MD 20771; email: tod.strohmayer@nasa.gov

ergs s^{-1} (e.g., Swartz et al. 2004 and references therein). The nature of the accretion process producing such high X-ray output is not completely understood, but there is now strong evidence supporting the notion that some of the brighter ULXs are accretion-powered systems containing a black hole. What remains more controversial is the mass of the accretor.

Current arguments suggest that these sources are either stellar-mass black holes (mass range: 3-50 $M_\odot$) emitting and/or accreting via a super-Eddington mechanism (e.g., Körding et al. 2002; King et al. 2001; Begelman et al. 2002), or that they comprise an intermediate-mass black hole (mass range: a few$\times$(100-1000)$M_\odot$) accreting at sub-Eddington accretion rates (Colbert & Mushotzky 1999). It is possible that the population of ULXs is an inhomogeneous sample powered by both mechanisms but, the controversy is far from resolved. The implications of the discovery of an intermediate-mass black hole are far-reaching. Most importantly, they are often required as building blocks to explain the formation of the super-massive black holes (Volonteri et al. 2003; Davies et al. 2011) that reside at the centers of almost all massive galaxies (Magorrian et al. 1998). The present work focuses on the ULX NGC 5408 X-1, one of the most promising candidates for an intermediate-mass black hole (Strohmayer et al. 2009). Here we present evidence for the detection of orbit-phase-dependent dips in its X-ray light curve that likely trace the orbital motion of the system. Similar phenomena have been studied in detail in the case of low-mass X-ray binaries (LMXBs).

There are now two detections of periodicities from long term X-ray monitoring of ULXs which may reflect orbital motion of these systems: a 62 day modulation in M82 X-1 detected with RXTE (Kaaret et al. 2007), and a 115.5 day period in NGC 5408 X-1 obtained from *Swift* data (Strohmayer 2009). Orbit-phase-dependent changes in the X-ray flux from accreting binaries can provide important insights as to the nature of the binary. For example, low-mass X-ray binaries (LMXBs) are X-ray sources where a compact object, either a black hole or a neutron star, accretes material from its companion star via Roche lobe overflow. To date, approximately 100 LMXBs have been identified (Ritter & Kolb 2003). A sub-sample of these sources, those accreting via Roche-lobe overflow and with their orbital planes suitably inclined to our line of sight, show periodic or quasi-periodic variations in their X-ray intensity. Such X-ray modulations have been well-studied (e.g., Parmar & White 1988; Mason 1986) and can be broadly classified into three categories: (1) periodic decreases in the X-ray flux due to *eclipsing* of the X-ray source by the companion star, (2) *smooth, quasi-sinusoidal* modulation in the X-rays, likely caused by the periodic obscuration of the extended X-ray source (usually referred to as the accretion disk corona) by vertical structures within the disk (White & Holt 1982), and (3) irregular, *sharp periodic/quasi-periodic dips* in the X-ray intensity. In the last case, the X-ray source is likely point-like, or has a significant point-like component, and the drop in the X-ray flux is again attributed to obscuration by vertical

structures in the accretion disk (White & Swank 1982; Walter et al. 1982; Frank, King & Raine 1987). It is also possible that a given source, depending on its inclination and the spatial extent of the X-ray source, as well as the accretion state, shows a combination of the above features in its X-ray light curve (e.g., Parmar et al. 1986; Parmar & White 1988). We will now discuss briefly each of the above scenarios.

Eclipsing of the X-ray source by the companion star is perhaps the most obvious X-ray signature of binary motion. Such eclipses are expected to be highly periodic and have a stable morphology, as the companion star evolves on time scales much longer than the orbital period. These properties are critical in distinguishing X-ray modulation due to eclipsing from the other two forms mentioned above. However, eclipses are expected only to be observed from binaries with favorably high inclinations (the exact value depends on the mass ratio of the binary). In such systems, the eclipses provide an excellent means to track the orbital motion of the companion star. Furthermore, a detailed study of the morphology of the eclipse can serve as an important diagnostic to measure certain systemic parameters, viz., the inclination of the orbit and the mass ratio of the binary components (e.g., Eggleton 1983; Rappaport & Joss 1983).

The other X-ray modulations observed from accreting compact binaries are the smooth quasi-sinusoidal variations and the sharp periodic/quasi-periodic dips. The physical medium responsible for both these modulations is the same. The basic idea is that there is an obscuring rim of varying height and density at a certain radius from the central X-ray source. As the X-ray source and hence the accretion disk orbits the center of mass of the binary, our line of sight intercepts different regions of the rim resulting in the observed X-ray modulation. Depending on whether the X-ray source is extended (accretion disk coronae: White & Holt 1982) or point-like, either smooth changes (quasi-sinusoidal) in the X-ray flux or sudden drops/dips (due to a local density enhancement in the rim) can occur, respectively. These modulations are expected to recur with the orbital period of the X-ray source which explains the apparent periodicity of the observed modulations. However, due to the turbulent nature of the accretion process and the irregularities in the disk material, these modulations may not be strictly periodic. Nevertheless, in most cases they provide a means to track the orbital motion of the X-ray source. Although the precise radial distance of such an obscuring rim from the center of the accretion disk is unclear (e.g., see Frank et al. 1987 for alternate locations of the rim), its origin is fairly well accepted. The fundamental hypothesis is that as the accretion stream from the companion star impacts the accretion disk it forms a bulge extending azimuthally along the outer edge (or at some inner radius, Frank et al. 1987) of the disk (e.g., Bisikalo et al. 2005). To summarize, a vertical structure in the accretion disk whose geometry is subject to disk inhomogeneities and turbulence is thought to be the primary source of the two observed X-ray modulations: quasi-sinusoidal X-ray modulations

and the periodic X-ray dips. These modulations provide a means to directly probe the orbital geometry.

Here we present a study of the X-ray monitoring data from NGC 5408 X-1 obtained to date with the *Swift* X-Ray Telescope (XRT). In particular, we present evidence for dips in the X-ray light curve and interpret the observed variability in the context of binary motion. The article is arranged as follows. In §2 we discuss the details of the *Swift*/X-ray telescope data used for this work. In §3 we study the long-term ($\sim$ a few hundred days) timing behavior of the source. In particular, we report the detection of the quasi-periodic X-ray dips along with the smooth, quasi-sinusoidal X-ray modulation. We derive the overall X-ray modulation profiles. We also present timing evidence (periodogram analysis) for a change in the physical properties of the system. In §4 we present energy spectral evidence for a change in the physical properties of the system. We also study the spectral differences between the dips and the non-dipping portions of the data. We discuss the implications of our results on the orbital motion of the X-ray source and the orbital inclination of the system in §5. We summarize our work in §6.

2. *Swift*/XRT Observations

The X-ray Telescope (XRT) onboard *Swift* began monitoring the ULX NGC 5408 X-1 in 2008 April as part of an approved Cycle 4 program (PI: Strohmayer). We include in our analysis all the observations obtained since the beginning of that program through 2011 August 30. The observing cadence has varied over this timespan of $\approx$ 3.4 yrs (1240 days), but on average the source was observed, when viewable, for a few ks once every 4 days. Gaps in the coverage due to *Swift* observing constraints occurred from 2008 September 26 - 2008 December 16 (81 days), 2009 September 25 - 2009 December 15 (81 days), 2010 September 26 - 2009 December 20 (85 days) and 2011 March 27 - 2011 May 1 (35 days). This provides a total of 305 pointed observations with a cumulative exposure of $\approx$ 500 ks distributed over a temporal baseline of $\approx$ 1240 days.

All the observations were carried out in the photon counting (PC) data mode. As noted earlier, these observations were spread over a time period of 1240 days. The XRT's CCD pixel structure and the calibration status also evolved during this period. Hence, to implement the most recent calibration files and to be able to account for the variations in the pixel structure, we began our analysis with the level-1 raw XRT event files (data as stored in the *Swift* archive). Each of the individual level-1 raw event files was reduced with the standard *xrtpipeline* data reduction tool. One crucial consideration during the reduction process was to mitigate the issue of bad pixels/columns on the XRT CCD. When a

source is positioned on such pixels, it can lead to an incorrect measurement of the flux. Furthermore, the bad pixels can result in an erroneous estimate of the response (effective area) of the instrument. The University of Leicester's XRT data analysis web page (http://www.swift.ac.uk/analysis/xrt/exposuremaps.php) provides a detailed discussion of this problem. The basic solution is to create exposure maps that account for the presence of bad pixels. We used *xrtexpomap* (*xrtpipeline* with the qualifier *xrtexpomap = yes*) to create exposure maps for each of the individual observations. These exposure maps were then used to correct the light curves (using *xrtlccorr*) and the ancillary response files (effective area) (using *xrtmkarf*) of each of the observations.

As recommended in the XRT's user guide, we only used events with grades 0 - 12 for further processing. We then used *XSELECT* to extract the light-curves and the energy spectra from the individual observations. We extracted source light-curves and spectra from a circular region of radius 47.1" centered around the source. This particular value was chosen to include roughly 90% (at 1.5 keV) of the light from the source (estimated from the fractional encircled energy of the XRT). A background region, free of other sources, was extracted in a nearby region. Given the low individual exposure times, to better estimate the background, we chose a circular region of twice the radius of the source, i.e., four times the source area. The same source and background region was used for extracting events from all the 305 observations. We present detailed timing and energy spectra analysis in the following sections.

3. Timing Analysis

This section is divided into four parts: (1) we show the complete ($\approx$ 1240 day temporal baseline) *Swift*/XRT X-ray (0.3-8.0 keV) light curve of NGC 5408 X-1, highlighting the most prominent features, (2) we compute periodograms (Lomb-Scargle) of two different portions of this complete light curve (one with strong quasi-sinusoidal X-ray modulation and the other with weak or absent modulation) showing evidence for a change in the physical nature of the source (which we further explore in the next section entitled energy spectrum analysis), (3) we extract an epoch folded light curve of the portion of the complete light curve with strong quasi-sinusoidal X-ray modulation for comparison with certain galactic binary sources and finally, (4) we study the energy dependence of the two distinct kinds of X-ray modulations detected, i.e., the quasi-sinusoidal modulation and the quasi-periodic dips.

3.1. X-ray Light Curve

As described in the previous section, between 2008 April and 2011 August *Swift* observed NGC 5408 X-1 on 305 occasions (for a few ks on each observation). For a given observation, we combined all the data to obtain an average source and background count rate. The light curve of the ULX NGC 5408 X-1 in the energy range of 0.3-8.0 keV is shown in Figure 1. The background countrate in the same energy range is also shown (red data points with black error bars). The background is almost always negligible compared to the source count rate. Roughly 40% of these observations, i.e., the first 113 observations of the present dataset, were analyzed by Strohmayer (2009) (S09 hereafter). The vertical line marked as S09 indicates the end of the observations used by S09 (see Figure 1). The main results of S09 are: (a) the discovery of a quasi-sinusoidal modulation of the X-ray flux with a period of 115.5±4 days and (b) that the amplitude of the modulation decreases with increasing energy. They interpreted the 115.5 day X-ray period to represent the periodic obscuration of an extended X-ray source by a vertical structure in the accretion disk, as the source exhibits orbital motion in an LMXB-like system. In other words, they concluded that the 115.5 day period might represent the orbital period of the binary.

However, the additional data provides new insights about the system. A prominent feature of the full light curve is the quasi-periodic recurrence of strong X-ray dips (though with non-zero X-ray intensity during the dips). These dips are highlighted with green circles in Figure 1. With the available temporal baseline of $\approx$ 1240 days, we detected five dips that recur roughly every 243 days. The exact time intervals between the dips are 251 days, 211 days, 276 days and 235 days. Given the variance in dip recurrence times, we can rule out partial eclipsing as the mechanism. Furthermore, these dips are strongly reminiscent of the periodic X-ray dips observed from high inclination galactic LMXBs (e.g., Parmar & White 1988; Mason 1986). If the dipping in NGC 5408 X-1 is indeed caused by the same phenomenon as in galactic LMXBs, i.e., periodic obscuration by a vertical structure in the accretion disk, then this indicates that the X-ray source in NGC 5408 X-1 is indeed in a binary, and the orbital period of the binary is likely $\approx$ 243 days as opposed to the 115.5 days reported by S09. In §5, we describe a possible geometry of the system (with two obscuring regions) to account for both the 115.5 day quasi-sinusoidal X-ray modulation and the X-ray dips that recur every 243 days. The second interesting feature that can be noted from Figure 1 is the higher frequency of dipping during the last continuous segment of the light curve. Also, although not as obvious, it can be seen from the light curve that the 115.5 day period X-ray modulation during the second half ($\approx$ last 600 days) of the light curve appears weaker compared to the first half ($\approx$ first 600 days) of the light curve. We argue that this might be due to a possible change in the physical nature of the system which we explore in the following section.

3.2. Timing Evidence for a physical change in the source

In this section we present timing evidence for a change in the physical behavior of the system. More specifically, we present evidence for weakening/disappearance of the 115.5 day quasi-sinusoidal X-ray modulation during the second half ($\approx$ last 600 days) of the light curve shown in Figure 1. The primary tool we use for this analysis is the Lomb-Scargle periodogram (Scargle 1982; Horne & Baliunas 1986). The precise location of the transition epoch is difficult to estimate. However, a closer look at the light curve (Figure 1) hints towards a weaker 115.5 day quasi-sinusoidal X-ray modulation in the second half of the light curve. Therefore, we started our analysis by dividing the light curve into roughly two equal segments. We then directly compared the Lomb-Scargle periodograms of the two segments of the light curve. We used all the photons in the energy range of 0.3-8.0 keV for this analysis. The two periodograms with their respective light curves are shown in Figure 2. The top left panel of the plot shows the light curve of the first half of the complete light curve (first half of Figure 1). The top right panel shows the Lomb-Scargle periodogram of this segment with confidence limits overlaid. The bottom left panel shows the light curve of the second half of Figure 1 (note the x-axis). The bottom right panel shows the periodogram of the second half of the complete light curve. The error bars on the power levels (y-axis) are negligible and are of the order of 1% (Scargle 1982). The highest peak in the periodogram of the first half of the light curve (top right panel of Figure 2) corresponds to a period of 112.6$\pm$4 days. This is consistent with the value reported by S09. Furthermore, such a peak is not evident in the periodogram of the second half of the data. We note that the reason for this difference cannot be purely statistical as the two portions of the light curve have comparable signal-to-noise ratios, temporal baseline ($\approx$ 600 days each) and sampling rate (with the exception of the last continous segment of the lightcurve which has a higher sampling rate of $\approx$ once per day). It is very likely that the drop in amplitude of the modulation in the second half of the light curve is physical. This is further supported with evidence from the differences in the energy spectra (see §4.1).

Furthermore, we suspect that the physical change in the system occurred roughly during the epoch indicated as "transition" in Figure 1. The reason for considering this particular location is twofold. The dipping phenomenon is much more pronounced and stochastic beyond this epoch compared to any other segment of the light curve. There is evidence in the case of galactic X-ray binaries that erratic dipping may be associated with state transitions (e.g., Naik et al. 2000; Naik et al. 2002; Díaz Trigo et al. 2006). Secondly, NGC 5408 X-1 was observed with *XMM-Newton* on multiple occasions (at least six observations with $\approx$ 100 ks/>100,000 counts each). These observations were distributed between 2006 January and 2011 January. Energy spectral analysis of these data sets revealed negligible change in the spectral parameters of the system (Strohmayer et al. 2009; Pasham & Strohmayer

2012, submitted). The long-term light curve (as in Figure 1) also does not show any drastic features (except the dips: more on this in the next section). It is therefore reasonable to assume that the source has remained in the same physical state at least through the end of the last of these high-quality *XMM-Newton* observations. The last of these observations were carried out only a few tens of days before the vertical line labeled transition. Therefore, the vertical line at $\approx$ 1130 days (Figure 1) serves as a reasonable indicator of the epoch during which the properties of the system may have changed.

3.3. Epoch folded light curve

Another simple, yet powerful tool to understand the nature of the modulation is epoch folding at a known period. In the case of NGC 5408 X-1, we have detected five dips prior to the transition epoch, i.e., the vertical line labeled as transition in Figure 1. If these dips are associated with the orbital period of the binary then the implied value of the orbital period is 243$\pm$23 days. The variance on this value is rather large. The precise value of the orbital period to use for folding the data is not known. Nevertheless, we folded the data at various values between $\approx$ 220-270 days, and then chose the value that resulted in the highest modulation amplitude. This value is 230 days.

Furthermore, for the purpose of obtaining a folded light curve, we considered only the data from the beginning to the vertical line marked as transition in Figure 1. This is because the modulation was weak and/or absent in the remainder of the light curve. To explore the dependence of the characteristic features in the folded light curve on the energy range, we folded the data from three energy bands. The resulting profiles are shown in Figure 3. All three panels show light curves folded at a period of 230 days. Each of these profiles were calculated with 26 phase bins per cycle and two cycles are shown for clarity. The top, middle and the bottom panel show the folded light curves using photons in the energy range from 0.3-8.0 keV (total *Swift*/XRT bandpass), 0.3-1.0 keV (soft band) and 1.0-8.0 keV (hard band), respectively. The most obvious features of these light curves are the quasi-sinusoidal X-ray modulation and the sharp X-ray dips. There are two peaks per cycle as expected (115.5 day quasi-sinusoidal period Vs the 230 day fold period). A quasi-sinusoidal function is overlaid on each of these folded light curves to guide the eye (dashed curves). We emphasize that these dashed curves do not represent model fits. Comparing the middle (folded light curve in the soft band) with the bottom (folded light curve in the hard band) panel, it appears that the quasi-sinusoidal modulation is weaker at higher energies, while the relative intensity during the dips (compared to the average countrate in that energy range) is energy independent, i.e., the ratio of the countrate of the dip to the average countrate in

the soft and the hard bands is $\approx 0.024/0.036$ (0.66) and $\approx 0.028/0.042$ (0.66), respectively. In the following section, we study the energy dependence of these two X-ray modulations in more detail.

3.4. Energy dependence of the two X-ray modulations

The band-limited epoch folded light curves (previous section) suggest that the quasi-sinusoidal X-ray modulation might be energy dependent while the X-ray dips might be energy independent. We systematically study the energy dependence of these two modulations in the following two sections.

3.4.1. Energy dependent quasi-sinusoidal X-ray modulation

Using only part of the present dataset, S09 reported that the amplitude of the quasi-sinusoidal X-ray modulation was energy dependent, with the modulation amplitude decreasing with increasing energy. Here we attempt to systematically quantify the variability as a function of the bandpass. The procedure we carry out is as follows. We obtain folded light curves in different energy bands. More specifically, keeping the upper limit of the bandpass constant at 8.0 keV, we vary the lower limit of the bandpass from 0.3 to 2.0 keV.

A few sample profiles with the best-fitting model (solid line) are shown in Figure 4. Again, two cycles are shown for clarity. Note that these profiles are the same as those shown in Figure 3 except for a difference in the number of bins per cycle. Here we used only 13 phase bins per cycle (compare to 26 phase bins in Figure 3) as our goal is to model only the overall quasi-sinusoidal modulation and not to study the subtle features within the modulation profiles. Again two cycles are shown for clarity.

To each of these profiles we fit a model that includes two Fourier components (the fundamental and the first harmonic), i.e., $I = A + B\sin 2\pi(\phi\text{-}\phi_0) + C\sin 4\pi(\phi\text{-}\phi_1)$. All the fits give acceptable values of reduced χ^2 (≈ 1 with 8 degrees of freedom). The fractional amplitude for such a model is defined as $f_{amplitude} = (max(I) - min(I))/(max(I) + min(I))$, and is an indicator of the amount of variability in the source in the given energy range. Figure 5 shows the variation of the fractional amplitude (y-axis) as a function of the lower limit of the energy considered (x-axis). Clearly, the fractional amplitude of the X-ray modulation is dependent on the energy range under consideration. The amplitude decreases with increasing energy. These results are consistent with those reported by S09.

3.4.2. Energy independent or dependent X-ray dips ?

To study the energy dependence of the X-ray dips, we extracted the hardness ratio during the dips and elsewhere. We define this as the ratio of the countrate in the hard band (1.0-8.0 keV) to the soft band (0.3-1.0 keV). The top panel of Figure 6 shows the hardness ratio as a function of time (in days). The middle and the bottom panels show the light curves in the soft (0.3-1.0 keV) and the hard (1.0-8.0 keV) bands, respectively. Owing to the lower count rates (compared to non-dip observations) during the dips, the error bars on the hardness ratio are especially large. It is not clear from these plots alone whether the X-ray dips from NGC 5408 X-1 are either energy independent or energy dependent. Obviously, longer exposures during the dips would be necessary to judge their true nature. In addition, the hardness ratio of the dips prior to the transition and after the transition are comparable. Within the error bars they seem consistent with each other. Therefore, to further aid our understanding of the nature of the dips, we extract and compare the combined energy spectrum of all the dips with the energy spectra derived from the non-dipping portions of the light curve (§4.2).

4. Energy spectral analysis

This section is mainly divided into two parts: (1) we investigate the differences in the energy spectra derived from two different portions of the complete light curve. We present spectral evidence for a change in the physical nature (the "transition") of the source and (2) we compare the average X-ray spectrum of the dips with the energy spectra derived from the non-dip observations, i.e., both the pre-transition and the post-transition spectra.

4.1. Energy spectral evidence for a physical change in the source

The timing analysis (§3.2) showed evidence that the source behaves differently during the first half of the data compared to the second half, i.e., the weakening/disappearance of the 115.5 day quasi-sinusoidal modulation and the presence of a significant number of X-ray dips during the second half of the light curve. More specifically, the epoch within the second half of the data where this transition likely occurred was also discussed (see Figure 1). In this section, we investigate the differences in the average energy spectra of the source before and after the transition epoch. For this purpose, we used only the non-dip observations, i.e., the observations with countrate (0.3-8.0 keV) greater than 0.05 counts sec^{-1}. Furthermore, the number of counts in each of the individual observations is too

low (a few 10s of counts) to extract a meaningful spectrum. However, since the source generally shows negligible variation in the energy spectrum until the transition epoch (Soria et al. 2004; Strohmayer et al. 2009; Pasham & Strohmayer 2012, submitted), we combined the data from all the observations until then to obtain an average pre-transition energy spectrum. Similarly, we extracted an average post-transition energy spectrum using all the non-dip observations carried out after the transition epoch. We used the FTOOL *sumpha* to combine the individual spectra. The two energy spectra in the X-ray energy range of 0.5-8.0 keV are shown in Figure 7. The average spectrum prior to the transition epoch is shown in black while the data from after the transition is shown in red. Both these spectra were binned to ensure a minimum of 50 counts in each spectral bin.

To quantify the spectra, we fit them with a model that is often used to describe the X-ray spectra of accreting black hole binaries: a multi-colored disk and a power law modified by photoelectric absorption. We used the XSPEC (Arnaud 1996) spectral fitting package to fit all our energy spectra. In terms of XSPEC models, we used *phabs*(diskpn+pow)*. The energy range we considered for spectral modeling was 0.6-8.0 keV. The X-ray spectrum of the dips (green points in Figure 7) suffers from significant statistical uncertainty below 0.6 keV. Therefore, we used the energy range of 0.6-8.0 keV for its spectral modeling. Now, to be consistent across all the X-ray spectra (as we will be comparing them directly with each other), we choose the same energy range to model the two non-dip energy spectra, i.e., the averaged pre-transition and the post-transition X-ray spectra.

Even without detailed modeling, it can be seen straightaway that there are significant differences between the two non-dip spectra at lower energies (below 1.5 keV). At energies below $\approx$ 1.5 keV, the dominant components of the current model (*phabs*(diskpn+pow)*) are the *phabs* (strong photoelectric absorption at lower X-ray energies) and the *diskpn* (the blackbody temperature peaks at $\sim$ 0.15 keV). Therefore, the apparent differences between the two spectra can either be due to a change in the absorption column density (*phabs*) or to changes in the disk properties, viz., disk temperature, and the disk normalization. The quality of the data does not allow us to independently constrain each model's parameters. To break this degeneracy, either one of the *diskpn* model parameters (the disk temperature or the disk normalization) or the column density had to be frozen. A careful analysis of the energy spectra reveals stronger statistical evidence for a varying column density than varying disk properties.

To illustrate this we simultaneously, but independently, fit the model to both the spectra (without freezing any model parameters except for the inner radius of the accretion disk). We then obtain confidence contours (χ^2) between the column densities, the disk temperatures and the disk normalizations of the pre-transition and the post-transition spectra. These

contours are shown in Figure 8. The top panel shows the confidence contours between the column density of hydrogen prior to the transition (X-axis) and after the transition (Y-axis). Similarly, the bottom left and the bottom right panels show the contours between the disk temperatures and the disk normalizations, respectively. In all the cases, the black, the red and the green represent the 1σ, 2σ and the 3σ confidence contours, respectively. In each case, the diagonal line shows the locus of points where the value on the X-axis equals the value on the Y-axis.

The amount of deviation of the confidence contours from this line indicates the significance of the variation of a given parameter between the pre-transition and the post-transition epochs. In other words, the larger the deviation the stronger is the evidence for a change in the given parameter. Clearly, the statistical evidence for an increase in the column density after the transition is very strong (top panel: strong deviation from the straight line) compared to that for changes in the disk temperature (bottom left panel) and the disk normalization (bottom right panel). In addition, the source has been observed on multiple occasions with *XMM/Newton* over the past ten years. The disk temperature on those occasions has remained essentially constant (Soria et al. 2004; Strohmayer et al. 2009; Pasham & Strohmayer 2012, submitted). Furthermore, in accreting galactic black hole binaries, changes in the accretion disk temperature are often accompanied by significant variations in the X-ray light curve (McClintock & Remillard 2006). Clearly, this is not seen in the light curve of NGC 5408 X-1. All the above analysis strongly suggests that the disk temperature has likely remained constant. Therefore, for subsequent analysis we assumed a constant disk temperature of 0.149 keV, the average value reported from the analysis of the high-quality *XMM-Newton* data (Pasham & Strohmayer 2012, submitted). The model then gives a reasonable fit in both cases (pre-transition and post-transition) with reduced χ^2 of 1.30 (179 degrees of freedom) and 1.29 (87 degrees of freedom). The best-fitting model parameters for the pre-transition and the post-transition non-dip spectra are shown in the first and the second row of Table 2, respectively.

The most prominent difference between the two spectra is the amount of photoelectric absorption. The total hydrogen column density before and after the transition epoch was $0.297^{+0.022}_{-0.022}\times10^{22}\mathrm{cm}^{-2}$ and $0.435^{+0.036}_{-0.040}\times10^{22}\mathrm{cm}^{-2}$, respectively. The post-transition X-ray spectrum is more absorbed than the pre-transition spectrum. The estimated total unabsorbed flux emitted in the energy range of 0.6-8.0 keV before the transition epoch and after the transition epoch is $3.68^{+0.21}_{-0.23}\times10^{-12}$ergs cm^{-2} s^{-1} and $6.71^{+0.70}_{-0.77}\times10^{-12}$ergs cm^{-2} s^{-1}, respectively. This suggests a factor of 2 increase in the unabsorbed X-ray flux during the last continuous segment of the light curve. Another important thing to note is the fraction of the disk contribution to the total flux before and after the transition epoch. The values are $1.69^{+0.28}_{-0.33}\times10^{-12}$ergs cm^{-2} s^{-1} and $4.55^{+0.89}_{-0.77}\times10^{-12}$ergs cm^{-2} s^{-1}, respectively. This implies

that the disk fraction of the total X-ray flux (0.6-8.0 keV) before and after the transition is $45.93^{+8.05}_{-9.42}$% and $67.81^{+15.03}_{-13.86}$%, respectively. In other words, the post-transition spectrum is more disk-dominated. This is important as X-ray state transitions in galactic X-ray binaries are often identified with the redistribution of the X-ray flux between the disk and the power law components (McClintock et al. 2009). It is therefore possible that NGC 5408 X-1 is also undergoing something like a state transition in the last continuous segment of the data. However, we caution that the evidence here is suggestive but not conclusive.

4.2. Dip spectrum vs Non-dip spectra

Owing to large uncertainties on the values of the hardness ratio, the X-ray dips prior to the transition epoch cannot be differentiated from the X-ray dips after the transition epoch. Furthermore, as discussed earlier, the individual observations have too few counts (several 10s) to extract a meaningful spectrum. This problem is even more pronounced during the dips where the countrate drops by a factor of ≈ 5 compared to the non-dip observations. Therefore, considering both these factors, i.e., comparable values of the hardness ratios (within the error bars) and to improve the signal-to-noise ratio of the energy spectrum, we combine all the dip observations to obtain an average dip spectrum. This spectrum is shown in Figure 7 (green data points) along with the two non-dip spectra. The dip spectrum was binned to ensure a minimum of 25 counts in each spectral bin. We fit the average dip spectrum with the same model (*phabs*(diskpn+pow)*) used to fit the non-dip spectra. The model gives a good fit with a reduced χ^2 of 1.00 (17 degrees of freedom). The best-fit parameters are shown in the last row of Table 2. The best-fit parameters of the energy spectrum of the dips are comparable to the values of the non-dip spectra. Again, owing to large error bars on the best-fit parameters, it is not clear whether there are any significant differences between the dip and the non-dip spectra.

5. Discussion & Implications

In this article we studied the X-ray (0.3-8.0 keV) properties of NGC 5408 X-1 using *Swift*/XRT monitoring over a temporal baseline of 1240 days. The primary results are: (1) the discovery of quasi-periodic dips in the X-ray intensity with an average recurrence period of 243 days and (2) evidence for a significant increase in the photoelectric absorption and a possible and timing transition at a certain epoch during the ≈ 1240 days of *Swift* monitoring. We now discuss the physical implications of these results.

As noted earlier, the X-ray light curves of certain accreting LMXBs, those inclined favorably to our line of sight, show periodic intensity modulations. The physical origin of a certain class of these modulations is thought to be due to the obscuration of the central X-ray source, either extended or point-like, by a distribution of azimuthally structured material within the disk. Now as the X-ray source orbits around the common center of mass, certain characteristic features in the X-ray light curve would repeat themselves over the timescale of the orbital period (White & Holt 1982; White & Swank 1982). In particular, one would expect to observe a quasi-sinusoidal modulation when the X-ray source is extended (comparable in size to that of the obscuring region), while sharp dips are expected when the X-ray emitting source is point-like. Ultimately, the modulation profile is determined by the overall distribution of the obscuring material within the disk and the spatial distribution of the X-ray source. In the case of NGC 5408 X-1, the data appear consistent with both these kinds of modulations, i.e., a quasi-sinusoidal modulation with a period of 112.6±4 days and sharp X-ray dips which recur on average every 243 days. Given that the source is very likely an accreting black hole, it is reasonable to assume that a similar physical mechanism may be responsible for the observed X-ray modulations. If so, then the most important implication is that NGC 5408 X-1 is in a binary orbit with an orbital period of 243±23 days.

5.1. Implications for the inclination of the binary orbit

The X-ray light curve of NGC 5408 X-1 presented here does not show obvious signs of eclipsing by the companion star, i.e., the observed dips are irregular and do not show the extremely periodic and regular variations expected from true eclipses. This can be interpreted in two ways: (1) If eclipses occur then their duration is shorter than the sampling time. In other words, it may be the case that we are missing the eclipses due to the coarse sampling of the observations or (2) the inclination of the source is such that true eclipses cannot be observed from this system.

Based on the current data it is not possible to completely rule out either scenario, however, we can place limits on the inclination of the system assuming that we are not missing the eclipses. Before we proceed to that calculation, we estimate a rough upper limit on the duration of the eclipses assuming we are missing them due to the observing cadence. Within the temporal baseline of 1240 days, the source was observed on 305 occasions. The observing cadence varied during different observing epochs. A simple plot of the histogram of the time interval between consecutive observations reveals three distinct peaks around 1.5 days, 3.5 days and 7 days. This indicates that the source was observed with three different sampling rates. The most conservative upper limit on the duration of an eclipse from this

source is therefore 7 days.

Now, assuming the second case, i.e., the inclination of the source is such that the eclipses cannot be observed, one can place upper limits on the inclination of the system. For this purpose we use the standard approximations to the radii of the Roche lobes of LMXBs (Eggleton 1983 and Rappaport & Joss 1986). Assuming that the compact source within NGC 5408 X-1 is powered by accretion via Roche lobe overflow of a companion star (similar to LMXBs), we can estimate the function connecting the duration of an eclipse, the inclination of the system and the mass ratio of the binary. This is given as follows,

$$(\cos^2 i + \sin^2 i \sin^2 \theta_e)^{1/2} = \frac{0.49q^{-2/3}}{0.6q^{-2/3}+\ln(1+q^{-1/3})}$$

where, i is the inclination of the binary orbit with respect to our line of sight, θ_e is the eclipse half angle defined as π times the fraction of the eclipse duration to the orbital period and q is the mass ratio (X-ray source to the companion star) of the X-ray binary. The left hand side of the equation is essentially a geometric approximation to the radius of the companion star (Rappaport & Joss 1986); while the right hand side is an approximation to the radius of a Roche lobe of the companion star (Eggleton 1983). Assuming the companion star fills its Roche lobe, one can equate both the radii. The allowed values of the inclination, assuming eclipses are not seen from this system, as a function of the mass ratio of the binary are shown in Figure 9. Currently, the mass estimate for the black hole within NGC 5408 X-1 is controversial, i.e., either a stellar mass black hole emitting at super-Eddington rate (Middleton et al. 2011) or an intermediate-mass black hole emitting at a sub-Eddington rate (Strohmayer et al. 2009; Pasham & Strohmayer 2012, submitted). Assuming the observed period of recurrence of the X-ray dips is indeed the orbital period of a Roche lobe filling binary, the density of the companion star can be constrained using the formula, $\rho \simeq 0.2(\mathrm{P}_{days})^{-2}$ g cm^{-3} (Frank et al. 2002). For a period of 243 days, this would imply that the companion star has a mean density of 3.4×10^{-6} g cm^{-3}. This value is consistent with a recent study by Grisé et al. (2012), who extracted the UV/optical/NIR spectral energy distribution (SED) of the optical counterpart of NGC 5408 X-1. The SED was consistent with that of a B0I supergiant star. The average mass of a B0 supergiant is $\approx 10\mathrm{M}_{\odot}$. If one were to assume that NGC 5408 X-1 hosts a massive stellar mass black hole (Middleton et al. 2011), say a mass of 10-50 $\mathrm{M}_{\odot}$ (mass ratio of 1-5), the upper limit on the systemic inclination is $\approx 70°$ (see Figure 9). However, if one were to assume that the source hosts an intermediate-mass black hole of a few $1000\mathrm{M}_{\odot}$ (Strohmayer et al. 2009, Pasham & Strohmayer 2012), i.e., a mass ratio of a few 100, this would relax the upper limit on the inclination to be $\approx 80°$-$85°$.

Additionally, if the dips are indeed caused by vertical structure within the disk, this would also support a high inclination (see, for example, Frank, King & Raine 1987). Within

the class of accreting X-ray binaries which show dips, two sources have independent measurements of their inclination. The cataclysmic variable GG Leo (J 1015+5417) has an inclination of 63°±12° (Ritter & Kolb 2003) and the LMXB GR Mus (XB 1254-690) has an inclination of 69°±4° (Ritter & Kolb 2003). Both these sources indeed have the relatively high values of inclination expected theoretically from dipping sources. If the observed dips in NGC 5408 X-1 are indeed associated with vertically structured obscuring material in the accretion disk, it is likely that this system also has a high value of inclination. Assuming the inclinations of the two X-ray dippers, GG Leo and GR Mus, to be representative of the typical inclinations of the population of X-ray dippers, and that we can rule out eclipses longer than about 7 days, we estimate the inclination of NGC 5408 X-1 to be $\gtrsim 60°$. It is worth noting that a high inclination further exacerbates the "luminosity problem" for a stellar-mass black hole. In other words, given the high inclination, the intrinsic luminosity of the source is atleast a factor of $(\cos i)^{-1}$ higher. This makes it more difficult, for models employing accretion onto a stellar-mass black holes, to explain the high X-ray output ($\sim(\cos i)^{-1} \times 10^{40}$ ergs s^{-1}) from NGC 5408 X-1.

The identification of an optical counterpart of NGC 5408 X-1 whose UV/optical/NIR SED is consistent with that of a B0I supergiant (Grisé et al. 2012) strengthens the argument that this system is likely an X-ray binary. While the X-rays dips in NGC 5408 X-1 are not strictly periodic, this is not inconsistent with the dipping behavior observed in galactic binaries, and can be attributed to the fact that the accretion process is turbulent (Lubow & Shu 1975) and any variation in the structure of the obscuring material within the accretion disk (responsible for X-ray dips) could cause the observed light curve to change. For example, the dipper X 1916-053, the first X-ray dipper discovered (Walter et al. 1982; Homer et al. 2001) and 4U 1624 - 49 (Smale et al. 2001) show variations in the morphology and recurrence time of dips from orbit to orbit. The point being that the obscuring material is not rigidly fixed within the binary and can vary on orbital timescales.

Furthermore, some galactic binaries also show two peaks per orbital cycle at certain times, similar to the two peak structure suggested by the NGC 5408 X-1 data presented here. The X-ray binaries, X1916-053 (Homer et al. 2001), X0748-676 (Parmar et al. 1988) and 4U 1822-37 (White et al. 1982) are sources where two peaks per orbital cycle have been seen. In those cases it has been suggested that the 2^{nd} peak per cycle could be due to tidal effects on the accretion disk, i.e., a second obscuring bulge region in the accretion disk (Ogilvie 2002). Given the strong similarity of the folded light curve, i.e., two peaks per cycle (see Figure 3), with some galactic binaries we suggest a physical scenario similar to the cases discussed above might be at work.

A schematic depiction of a possible source geometry is shown in Figure 10. The top

panel shows an overhead view of the binary. The absolute phase information is not known (ϕ here is a constant offset whose value is unknown). The schematic shows two obscuring regions along the accretion disk rim that could in principle account for the double-peaked nature of the light curve; one associated with the region of accretion stream impact, and the other approximately half a cycle away. The middle panel shows the light curve folded at 230 days (same as Figure 3) while the bottom panel shows an idealized view of the possible azimuthal distribution of the obscuring material along the rim of the accretion disk. As in the case of LMXBs, the smooth quasi-sinusoidal modulation detected here is likely at least partly due to the presence of an extended X-ray source, i.e, an accretion disk corona (ADC). The circular region on the left of the bottom half of the bottom panel represents the putative ADC. As the X-ray source orbits the common center of mass (as the ADC moves to the right in the bottom half of the bottom panel), the amount of obscuring material changes giving rise to the observed modulation profile. The X-ray dips are likely due to local density enhancements (represented by the dense bulge at phase 0.7). In summary, we suggest that the X-ray modulations observed from NGC 5408 X-1 are comparable to those seen in accreting X-ray binaries. The variations in the dip-recurrence period and the presence of two peaks per cycle can be attributed to the dynamic nature of the accretion process and the presence of a secondary, tidally-produced bulge, respectively (Ogilvie 2002).

The energy dependence of the observed modulations can provide clues as to the nature of the absorbing/obscuring material. More specifically, it was noted above (see Figures 4 & 5) that the amplitude of the quasi-sinusoidal modulation was decreasing with increasing energy, i.e., higher amplitude at lower energies (< 1.0 keV). This can be accommodated if, for example, absorption or scattering is more efficient at lower energies. We might then expect the dip spectrum to show evidence for a higher absorbing column, but this is not conclusive due to the low number of photons present during the dips. Nevertheless, the fact that the column depth does not appear dramatically higher in the dips suggests that a combination of both absorption and scattering is likely involved in producing the observed modulations. This then suggests at least partial ionization of the obscuring/scattering material, and would not be unexpected given the high source luminosity.

5.2. Alternative Scenarios

Alternatively, it could be that the observed X-ray modulations from NGC 5408 X-1 are not due to orbital motion of the X-ray source in a binary (Foster et al. 2010). X-ray modulations on "super-orbital" periods (periods longer than the binary orbital period) of the order of a few days to a few hundred days have been reported from accreting X-ray binaries

(e.g., Wen et al. 2006; Sood et al. 2007). In a sub-sample of these sources consisting of Her X-1 ($P_{Superorbit} = 35$ days), SS 433 ($P_{Superorbit} = 164$ days), LMC X-4 ($P_{Superorbit} = 30.4$ days) and SMC X-1 ($P_{Superorbit} \approx 55$ days), it is likely that the observed X-ray modulation is due to the periodic obscuration of the central X-ray source by a tilted, precessing accretion disk. The basic idea here is that the accretion disk is tilted with respect to the orbital plane of the binary. The tidal effects of the companion star then force the accretion disk to precess about an axis normal to the binary orbit. As the tilted disk precesses, the effective area of the disk obscuring the central X-ray source can vary, producing modulations at or near the precession period. Furthermore, the tidal force of the companion star can warp the outer regions of the accretion disk (Ogilvie & Dubus 2001; Ogilvie 2002) leading to two spatially distinct density enhancements. This might possibly account for the twin-peaked X-ray modulation curve of NGC 5408 X-1. In summary, the theory of tilted, warped accretion disks can likely be adapted to the present scenario to perhaps explain the observed properties.

5.3. Interpretation of the observed change in the physical state of the system

In the previous sections, we carried out timing (Lomb-Scargle periodograms) and energy spectral analysis (spectral modeling) of two different portions of the complete 1240 day X-ray light curve of NGC 5408 X-1. We found significant changes in the timing and energy spectral properties of the source during these two different segments of the data. The primary differences we identified were: (1) the appearance of more erratic dips during the last continuous segment of the light curve (see Figure 1), (2) a decrease/disappearance of the quasi-sinusoidal X-ray modulation during the second half of the data (see Figure 2), (3) a significant increase in the photoelectric absorption during the last continuous segment of the data (compare the red and black spectra of Figure 7), and (4) an increase in the disk contribution to the total flux (67% compared to 45%) during the last continuous segment of the data. These results suggest the source may have experienced a physical change during a certain epoch of the *Swift* monitoring program.

Possible explanations that might address these observations are an increase in the mass accretion rate onto the compact object and perhaps a change in the ionization state of the circumbinary material. More specifically, the apparent erratic dipping in the last portion of the light curve is suggestive of the presence of more obscuring material within the accretion disk, and this could also account for the higher column density. The spectral analysis suggests a modest increase in the disk flux component as well, also suggestive of a higher accretion rate. If the column depth from the X-ray source to the obscuring regions in the outer disk is increased this would also likely affect the ionization balance, which could also influence the

filling factor of absorbtive material capable of producing dips.

Moreover, if absorption and scattering is increasing in the vicinity of and after the epoch of transition, then additional scattering could in principle affect the observed modulation amplitude (Miller 2000, and references therein), perhaps contributing to the apparent decrease of the quasi-sinusoidal modulation amplitude in the latter portions of the light curve. To fully address these issues would require more extensive physical modeling which is beyond the scope of this paper.

6. Summary

We present results from long-term (305 pointings over 1240 days with an average of a few ks per observation) X-ray (0.3-8.0 keV) monitoring of the ULX NGC 5408 X-1 using *Swift*/XRT. Our primary results are: (1) the discovery of dips (a total of 5 dips) in the X-ray intensity that recur roughly every 243 days and (2) the detection of a smooth, quasi-sinusoidal modulation of the X-rays which disappears/weakens during the second half of the monitoring program. It is possible that these findings reveal the orbital motion of the X-ray source in a Roch-lobe overflow binary with a period comparable to the dip-recurrence period (243±23 days). Assuming this to be the case, we suggest a possible geometry of the system that can explain both the observed X-ray modulations, i.e., the quasi-sinusoidal modulation and the quasi-periodic dips. A schematic of this scenario is shown in Figure 10. While it is also possible that a precessing accretion disk (a non-orbital phenomenon) can cause a similar X-ray modulation, it should be noted that NGC 5408 X-1 is one of only two ULXs (the other being M82 X-1: Kaaret & Feng 2007; there is some evidence of a 6.1 day optical photometric period from NGC 1313 X-2; Liu et al. 2009) known to show any kind of statistically significant periodicity. If the observed periodicity is indeed orbital, it provides a means to directly measure the mass of the binary companion and hence the black hole itself. Finally, we suggest that further X-ray monitoring of NGC 5408 X-1 be continued, as for example, with *Swift* to firmly establish that the X-ray dips are indeed associated with the orbital period of the binary.

REFERENCES

Arnaud, K. A. 1996, Astronomical Data Analysis Software and Systems V, 101, 17

Begelman, M. C. 2002, ApJ, 568, L97

Bisikalo, D. V., Kaigorodov, P. V., Boyarchuk, A. A., & Kuznetsov, O. A. 2005, Astronomy Reports, 49, 701

Colbert, E. J. M., & Mushotzky, R. F. 1999, ApJ, 519, 89

Davies, M. B., Miller, M. C., & Bellovary, J. M. 2011, ApJ, 740, L42

Díaz Trigo, M., Parmar, A. N., Boirin, L., Méndez, M., & Kaastra, J. S. 2006, A&A, 445, 179

Eggleton, P. P. 1983, ApJ, 268, 368

Foster, D. L., Charles, P. A., & Holley-Bockelmann, K. 2010, ApJ, 725, 2480

Frank, J., King, A. R., & Lasota, J.-P. 1987, A&A, 178, 137

Frank, J., King, A., & Raine, D. J. 2002, Accretion Power in Astrophysics, by Juhan Frank and Andrew King and Derek Raine, pp. 398. ISBN 0521620538. Cambridge, UK: Cambridge University Press, February 2002.,

Grisé, F., Kaaret, P., Corbel, S., et al. 2012, ApJ, 745, 123

Homer, L., Charles, P. A., Hakala, P., et al. 2001, MNRAS, 322, 827

Horne, J. H., & Baliunas, S. L. 1986, ApJ, 302, 757

Kaaret, P., & Feng, H. 2007, ApJ, 669, 106

King, A. R., Davies, M. B., Ward, M. J., Fabbiano, G., & Elvis, M. 2001, ApJ, 552, L109

Körding, E., Falcke, H., & Markoff, S. 2002, A&A, 382, L13

Lewin, W. H. G., & van den Heuvel, E. P. J. 1983, Accretion-Driven Stellar X-ray Sources,

Liu, J., Bregman, J. N., & McClintock, J. E. 2009, ApJ, 690, L39

Lubow, S. H., & Shu, F. H. 1975, ApJ, 198, 383

Magorrian, J., Tremaine, S., Richstone, D., et al. 1998, AJ, 115, 2285

Mason, K. O. 1986, The Physics of Accretion onto Compact Objects, 266, 29

McClintock, J. E., & Remillard, R. A. 2006, Compact stellar X-ray sources, 157

McClintock, J. E., Remillard, R. A., Rupen, M. P., et al. 2009, ApJ, 698, 1398

Middleton, M. J., Roberts, T. P., Done, C., & Jackson, F. E. 2011, MNRAS, 411, 644

Miller, M. C. 2000, ApJ, 537, 342

Naik, S., & Rao, A. R. 2000, A&A, 362, 691

Naik, S., Rao, A. R., & Chakrabarti, S. K. 2002, Journal of Astrophysics and Astronomy, 23, 213

Ogilvie, G. I., & Dubus, G. 2001, MNRAS, 320, 485

Ogilvie, G. I. 2002, MNRAS, 330, 937

Parmar, A. N., & White, N. E. 1988, Mem. Soc. Astron. Italiana, 59, 147

Parmar, A. N., White, N. E., Giommi, P., & Gottwald, M. 1986, ApJ, 308, 199

Pasham, D. R., Strohmayer, T. E. 2012, ApJ, submitted

Ritter, H., & Kolb, U. 2003, A&A, 404, 301

Scargle, J. D. 1982, ApJ, 263, 835

Smale, A. P., Church, M. J., & Bałucińska-Church, M. 2001, ApJ, 550, 962

Sood, R., Farrell, S., O'Neill, P., & Dieters, S. 2007, Advances in Space Research, 40, 1528

Soria, R., Motch, C., Read, A. M., & Stevens, I. R. 2004, A&A, 423, 955

Strohmayer, T. E., & Mushotzky, R. F. 2009, ApJ, 703, 1386

Strohmayer, T. E. 2009, ApJ, 706, L210

Swartz, D. A., Ghosh, K. K., Tennant, A. F., & Wu, K. 2004, ApJS, 154, 519

Volonteri, M., Haardt, F., & Madau, P. 2003, ApJ, 582, 559

White, N. E., & Holt, S. S. 1982, ApJ, 257, 318

White, N. E., & Swank, J. H. 1982, ApJ, 253, L61

Walter, F. M., Mason, K. O., Clarke, J. T., et al. 1982, ApJ, 253, L67

Wen, L., Levine, A. M., Corbet, R. H. D., & Bradt, H. V. 2006, ApJS, 163, 372

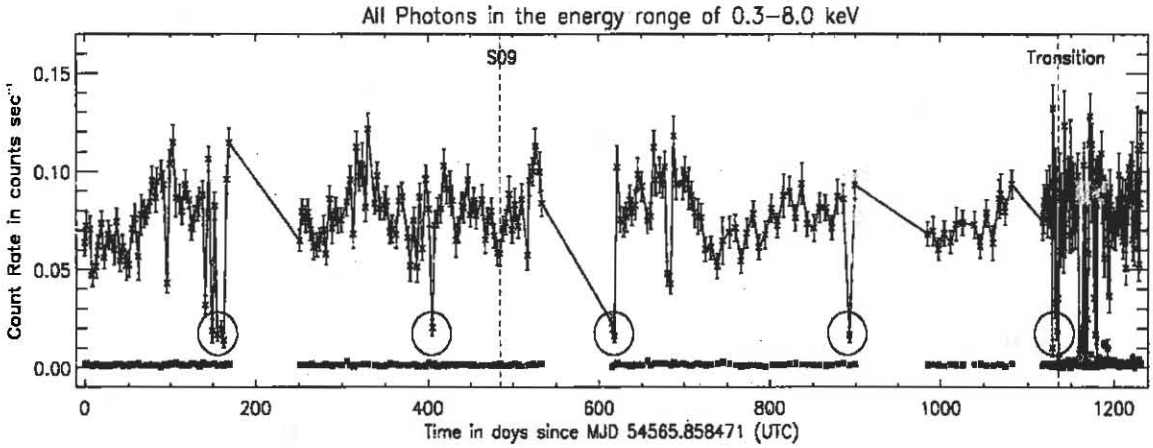

Figure 1: The *Swift*/XRT X-ray light curve of the ULX NGC 5408 X-1 in the energy range 0.3-8.0 keV. The background count rates with their respective error bars are also shown (red points and black error bars within). The most prominent feature of the light curve is the quasi-periodic recurrence of the dips. These are highlighted with green circles. The vertical line labeled as S09 marks the last observation used by Strohmayer et al. (2009). The vertical line labeled as "transition" corresponds to the approximate epoch at which the physical properties of the system may have changed (see text). Time zero corresponds to MJD 54565.85847 (UTC).

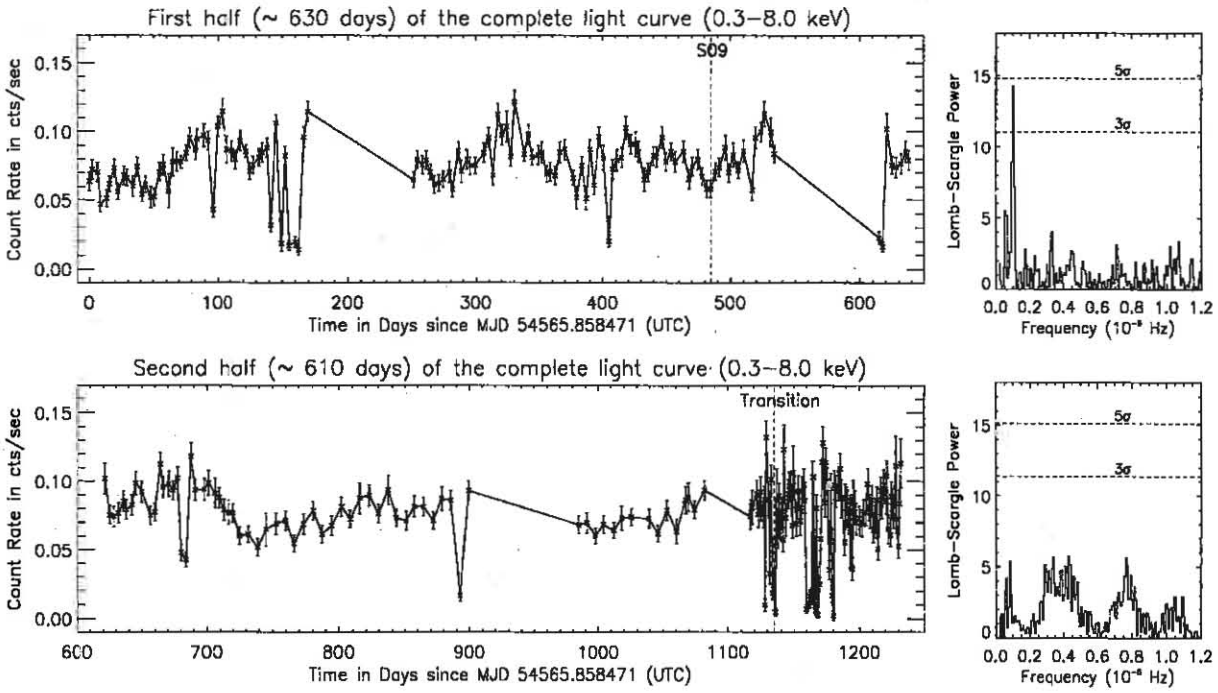

Figure 2: *Top Left Panel:* First half ($\approx$ 630 days) of the complete *Swift*/XRT X-ray light curve of the ULX NGC 5408 X-1 in the energy range 0.3-8.0 keV. *Top Right Panel:* The Lomb-Scargle periodogram of the first half of the *Swift*/XRT X-ray light curve of NGC 5408 X-1 (top left panel). The highest peak corresponds to 112.6$\pm$4 days. *Bottom Left Panel:* Second half ($\approx$ 610 days) of the *Swift*/XRT X-ray light curve of the ULX NGC 5408 X-1 in the energy range 0.3-8.0 keV. Note the erratic dipping in the last continuous segment of the data. *Bottom Right Panel:* The Lomb-Scargle periodogram of the second half of the complete *Swift*/XRT X-ray light curve of NGC 5408 X-1 (bottom left panel). Note the difference between the two periodograms: there is no statistically significant period detected during the second half of the light curve.

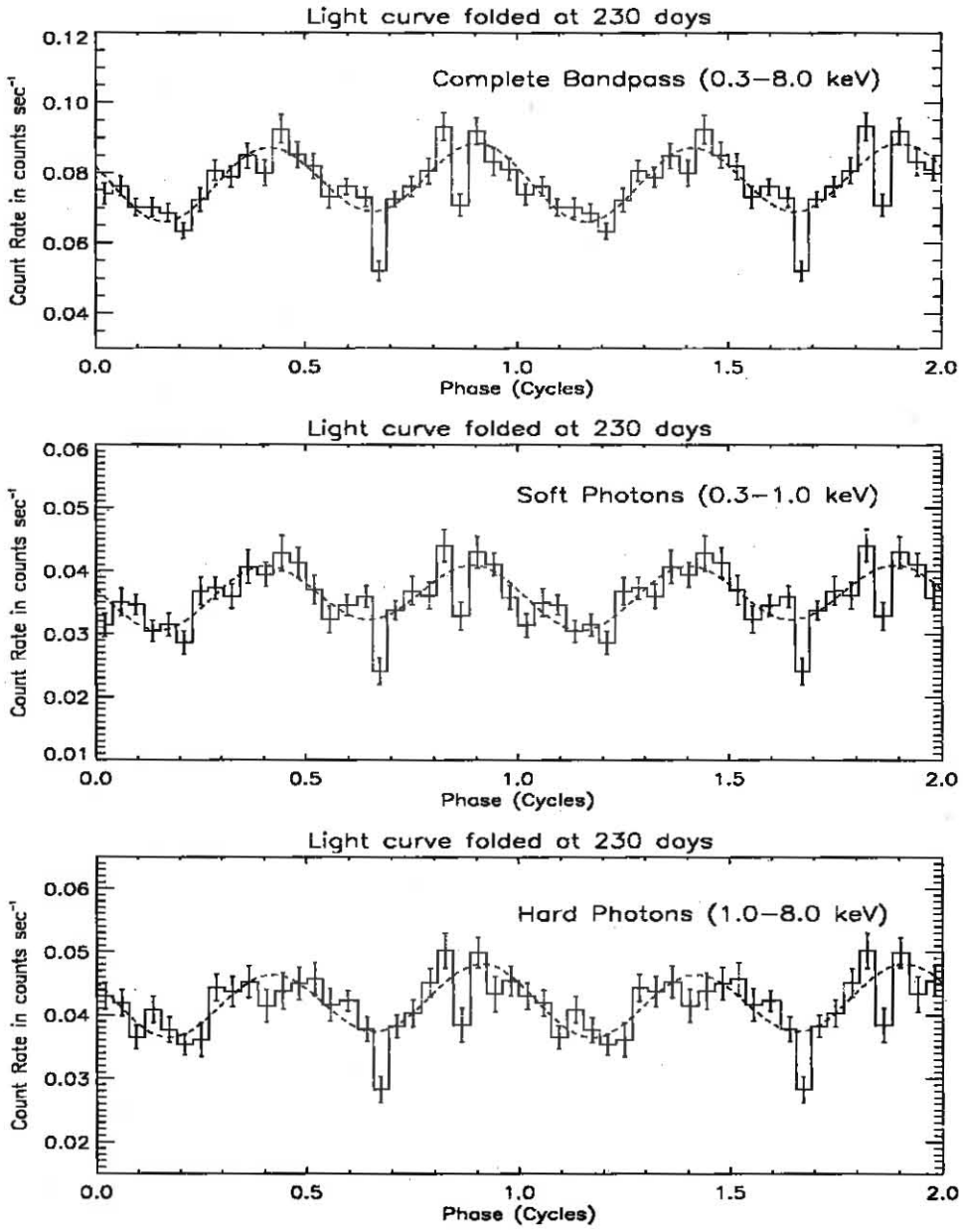

Figure 3: The epoch folded light curve of NGC 5408 X-1 in three energy bands. All the light curves are folded at a 230 day period. We used 26 phase bins per cycle and two cycles are shown for clarity. A quasi-sinusoidal curve is overlaid on each of the profiles. We emphasize that these curves are *not* best-fitting models. Their purpose here is only to guide the eye. *Top Panel:* The folded light curve using photons in the energy range of 0.3-8.0 keV. *Middle Panel:* The folded light curve in the soft band (0.3-1.0 keV). *Bottom Panel:* The folded light curve in the hard band (1.0-8.0 keV). Two types of X-ray modulation are evident: (1) quasi-sinusoidal X-ray variations (two peaks per cycle) and (2) sharp X-ray dips. The quasi-sinusoidal modulation appears to be weaker in the hard band while the X-ray dips appear to be energy independent.

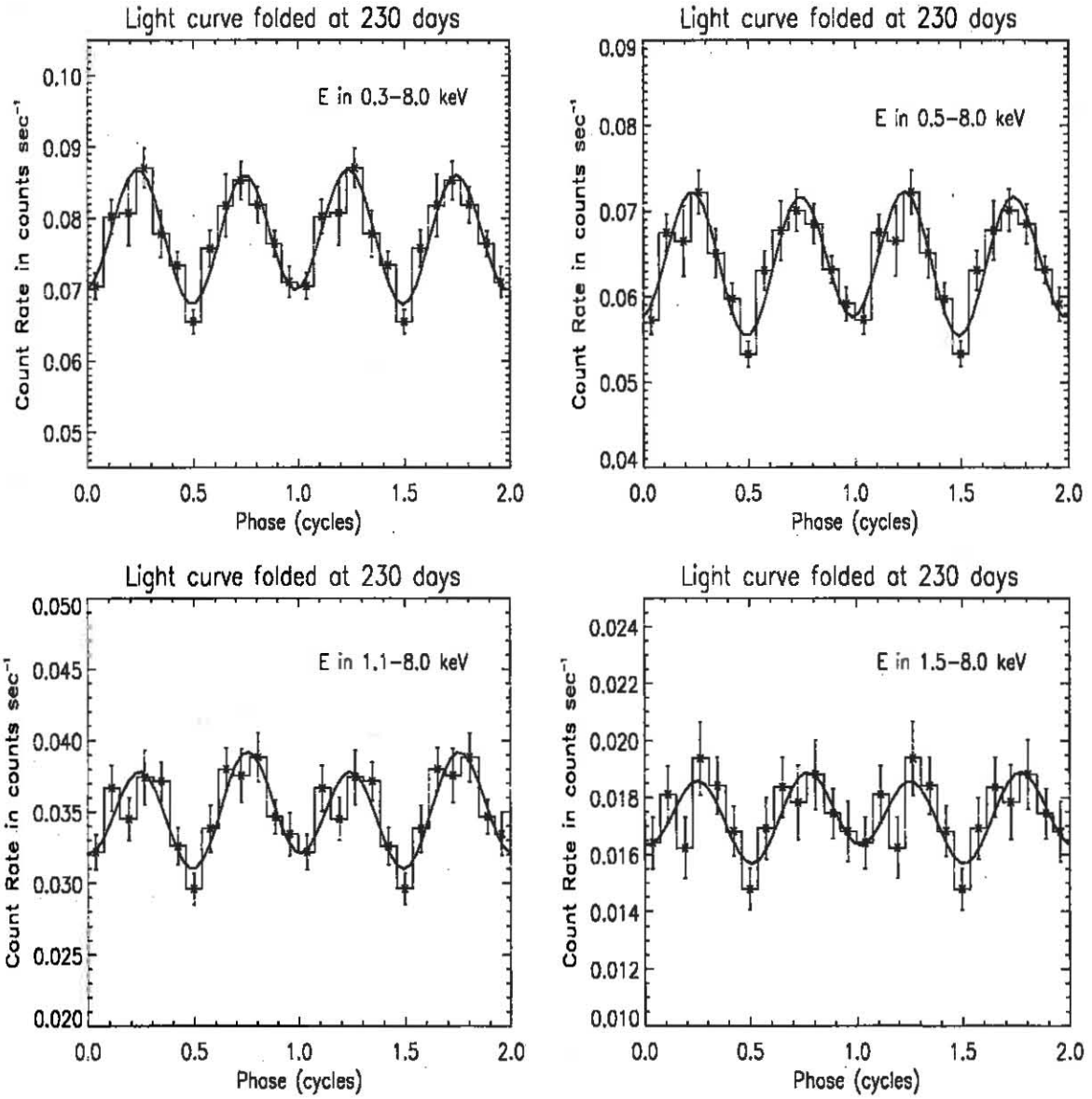

Figure 4: The epoch folded light curves of NGC 5408 X-1 in varying energy bands. The light curves in the energy range 0.3-8.0 keV, 0.5-8.0 keV, 1.1-8.0 keV and 1.5-8.0 keV are shown in the top left, top right, bottom left and the bottom right panels, respectively. In each case, we used 13 phase bins per cycle and two cycles are shown for clarity. To each of these profiles we fit a model that includes two Fourier components (the fundamental and the first harmonic), i.e., $I = A + B\sin 2\pi(\phi\text{-}\phi_0) + C\sin 4\pi(\phi\text{-}\phi_1)$. The best fitting curve is overlaid (solid curve). Clearly, the modulation amplitude decreases with increasing energy.

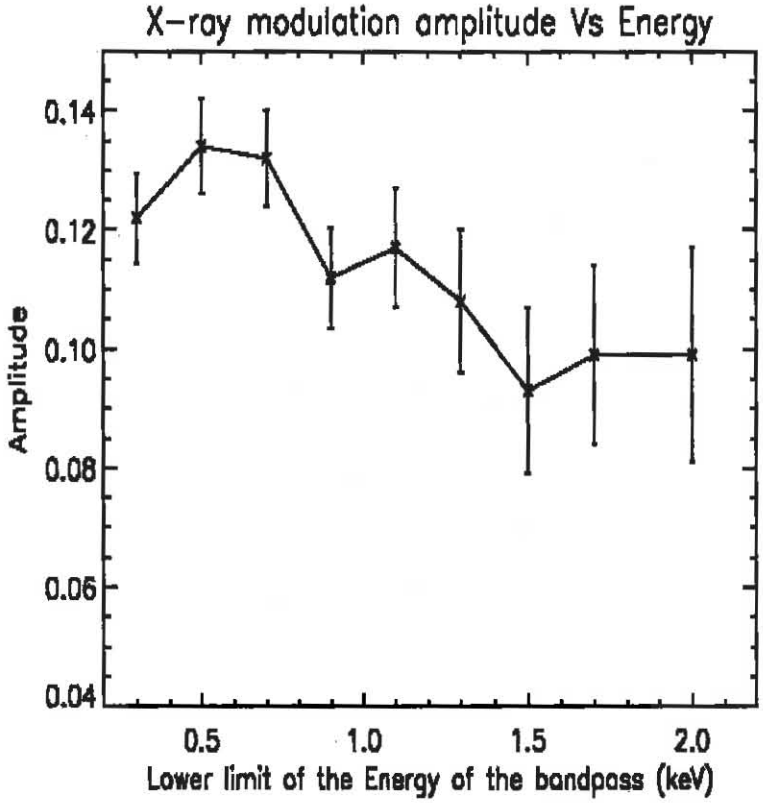

Figure 5: The fractional amplitude of the X-ray modulation as a function of the lower limit of the band pass is shown. The upper limit of the bandpass was fixed at 8 keV. The fractional amplitude of the mathematical form used to model the epoch folded light curves of NGC 5408 X-1 (Figure 4) is defined as $f_{amplitude} = (max(I) - min(I))/(max(I) + min(I))$. Clearly, the amplitude of the quasi-sinusoidal modulation decreases with increasing energy.

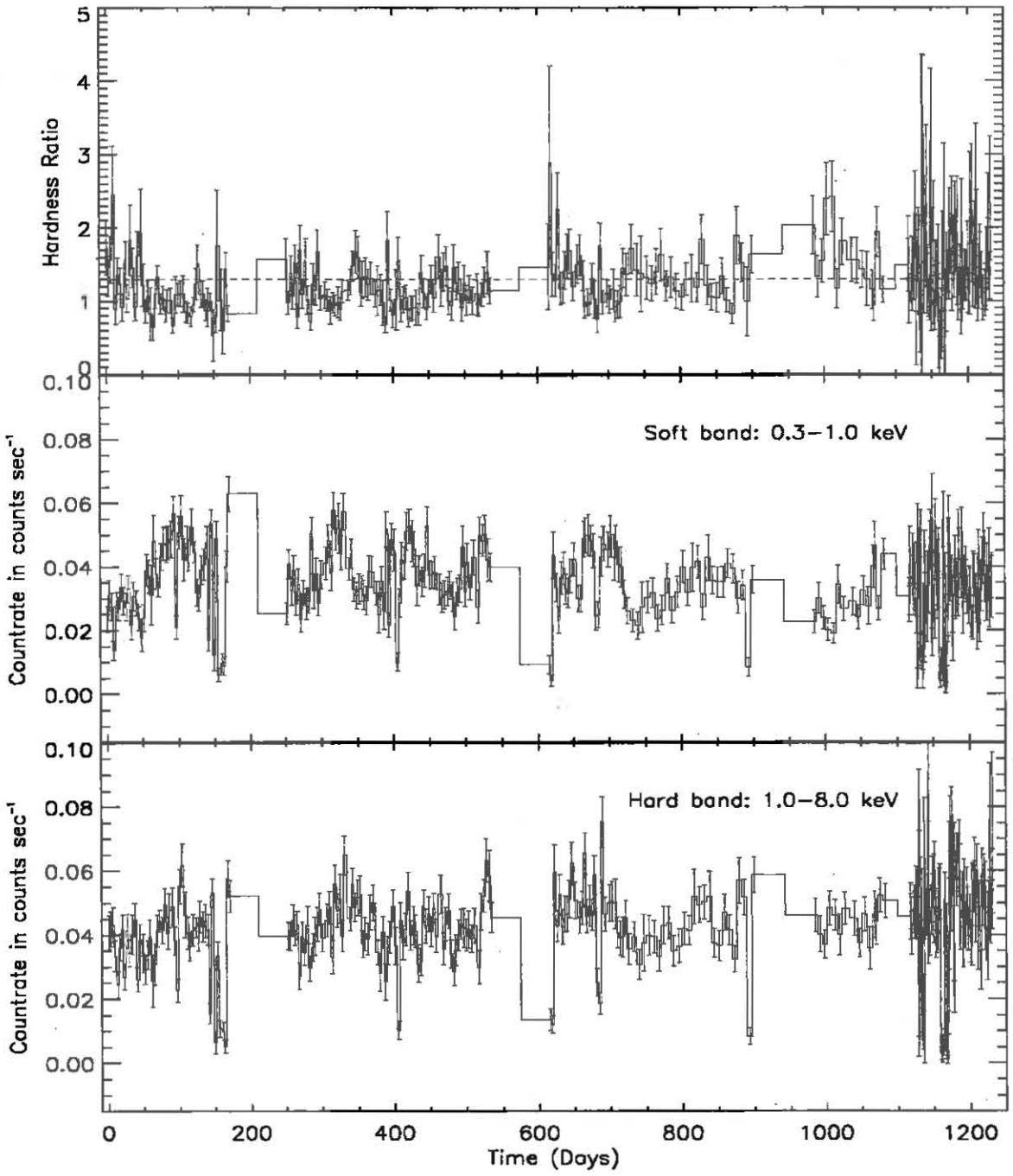

Figure 6: *Top panel:* Time history of the hardness ratio (ratio of the count rate in the hard band (1.0-8.0 keV) to the soft band (0.3-1.0 keV)). The mean value is indicated by the dashed line. *Middle panel:* The light curve of the source in the soft band, i.e., 0.3-1.0 keV. *Bottom panel:* The light curve of the source in the hard band, i.e., 1.0-8.0 keV.

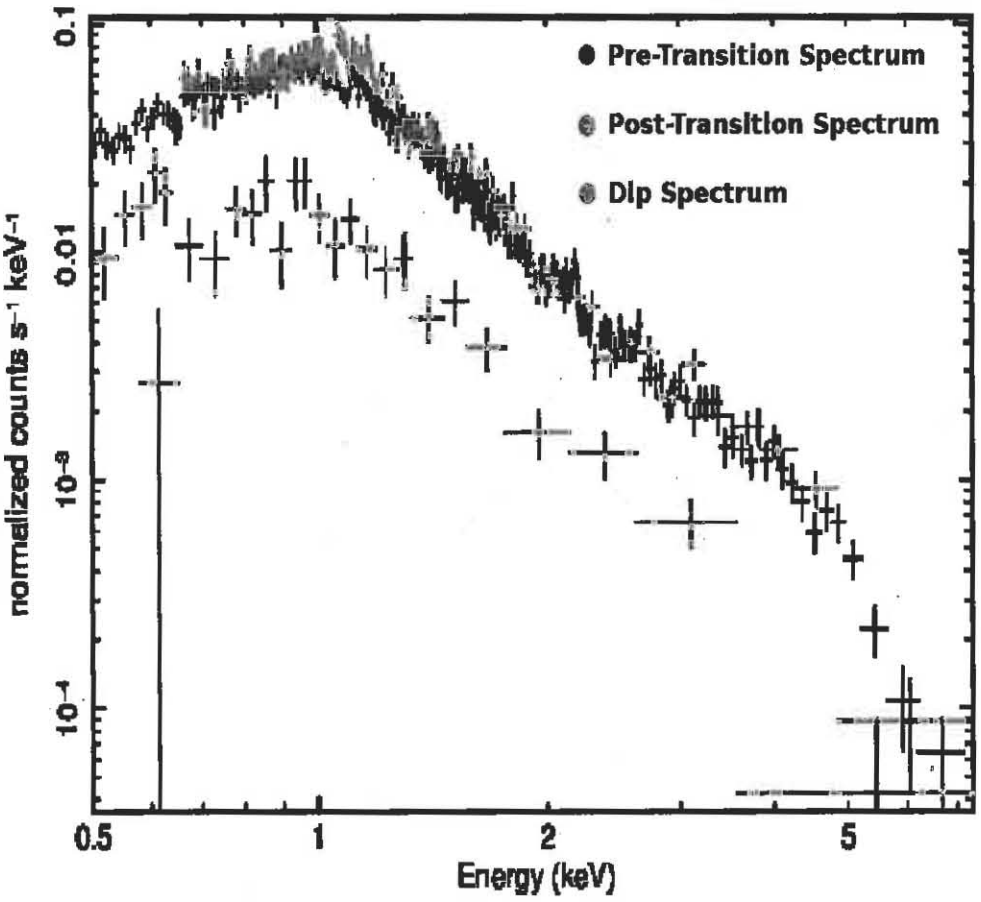

Figure 7: The *Swift*/XRT energy spectra of NGC 5408 X-1 in the energy range 0.5-8.0 keV. The *black* points show the average non-dip energy spectrum prior to the transition epoch (as marked by the vertical line in Figure 1). Shown in *red* is the average non-dip energy spectrum of the source after the transition epoch. The *green* data points denote the average energy spectrum during the dips. The two non-dip spectra, i.e., the pre-transition and the post-transition spectra, are binned to ensure a minimum of 50 counts per spectral bin, while the dip-spectrum is binned to ensure a minimum of 25 counts per spectral bin. There are clear differences between the two non-dip spectra, especially at lower energies (below 1.5 keV).

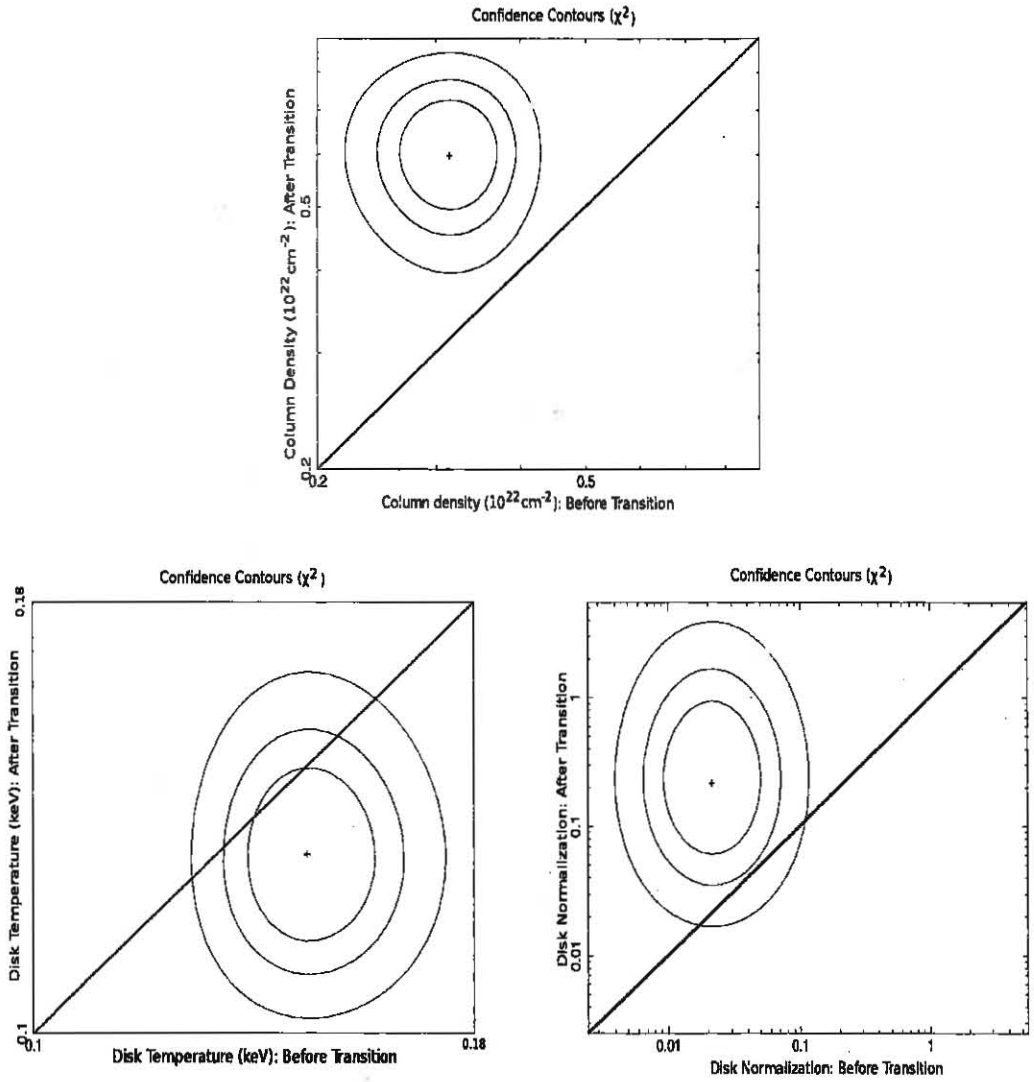

Figure 8: *Top Panel:* The confidence contours of the total hydrogen column densities along the line of sight (n_H) before (X-axis) and after (Y-axis) the transition epoch. *Bottom Left Panel:* The confidence contours of the disk temperatures before (X-axis) and after (Y-axis) the transition epoch. *Bottom Right Panel:* The confidence contours of the disk normalizations before (X-axis) and after (Y-axis) the transition epoch. The black, red and the green curves in each panel represent the 1σ, 2σ and the 3σ confidence contours. The straight line in each case represent the locus of all points with X = Y. For a given parameter, if the contours do not overlap with this line then that is a strong indication for a change in the parameter value.

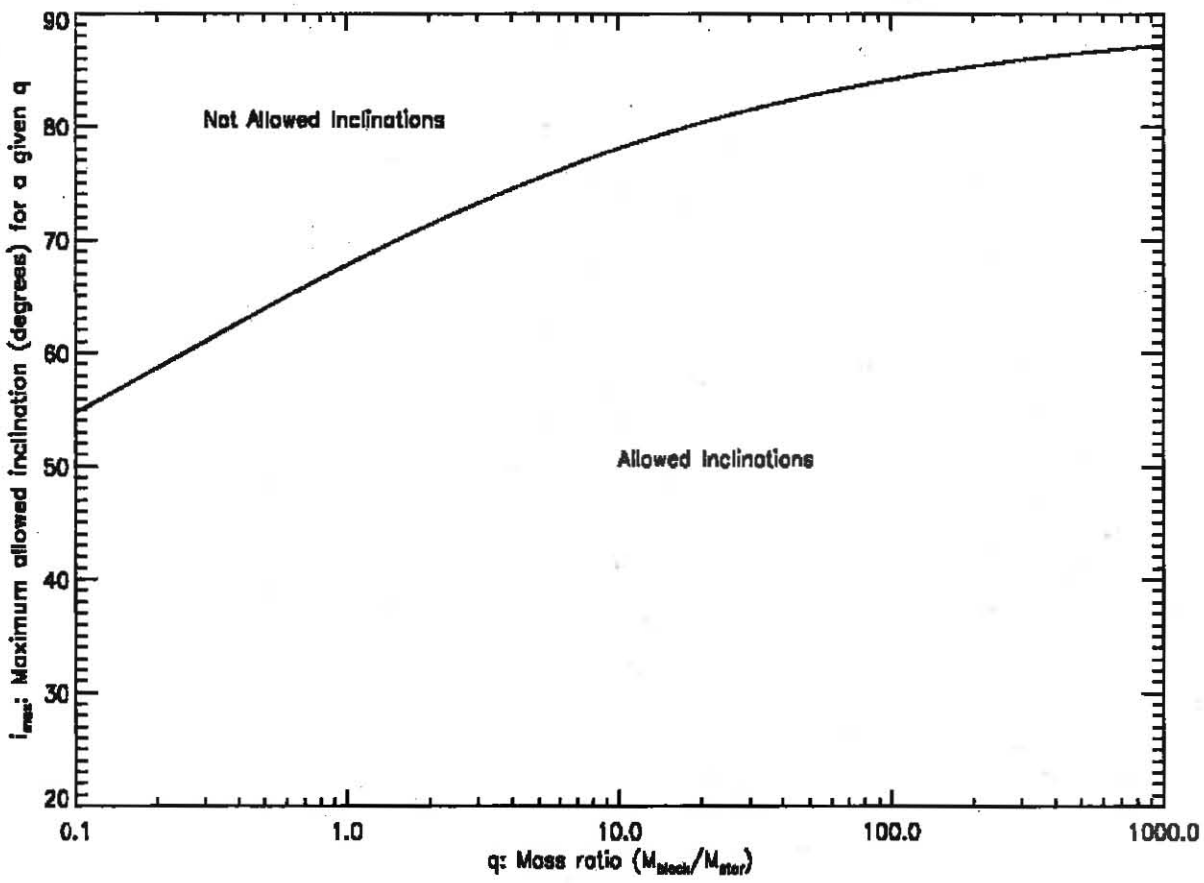

Figure 9: Maximum allowed inclination as a function of the mass ratio of the binary assuming eclipses have not been missed due to the temporal sampling. The optical counterpart is consistent with being a B0I supergiant (Grisé et al. 2012 , mass $\approx 10M_{\odot}$). Assuming the source is powered by a stellar-mass black hole and an intermediate-mass black hole ($\sim$ a few $100M_{\odot}$), the upper limits on the inclination are $\approx 70°$ and $\approx 80°$-$85°$, respectively.

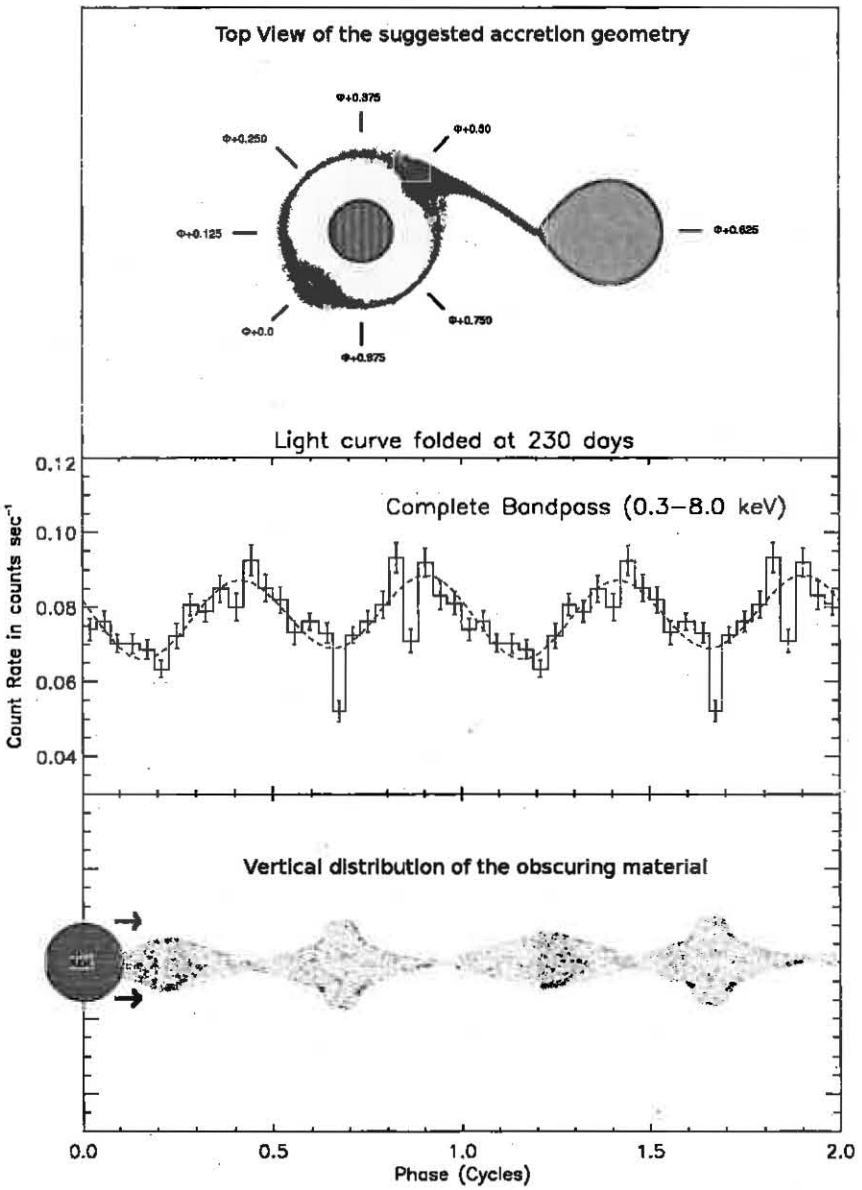

Figure 10: *Top panel:* An idealized depiction of a possible accretion geometry for NGC 5408 X-1. The optical star (possibly a B0I supergiant, Grisé et al. 2012) is shown in blue (right), while the accretion disk with two obscuring regions is shown on the left hand side. The observed quasi-sinusoidal modulation could be due to the presence of an extended X-ray source. This is represented by the central circular region of the accretion disk. The absolute phase information is not known. An arbitrary offset, ϕ, is shown to indicate this. *Middle panel:* light curve of the source folded at a period of 230 days. Notice the two peaks per cycle and the sharp dips. *Bottom panel:* An idealized edge-on view of the vertical distribution of the obscuring material that could explain the observed light curve. The motion of the extended X-ray source around the center of mass is equivalent to the motion of the X-ray emitting region across the circumferential distribution of the obscuring material.

Table 1: Summary of the best-fitting model parameters of the X-ray modulation profiles of NGC 5408 X-1

Bandpass (keV)	A[1] (10^{-2})	B[1] (10^{-2})	ϕ_0^1	C[1] (10^{-2})	ϕ_1^1	f[2] $_{amplitude}$	χ^2/dof
0.3-8.0	7.77 ± 0.05	0.11 ± 0.06	0.80 ± 0.15	-0.88 ± 0.07	0.87 ± 0.01	0.122 ± 0.015	8.89/8
0.5-8.0	7.51 ± 0.05	0.12 ± 0.07	0.87 ± 0.12	-0.92 ± 0.07	0.87 ± 0.01	0.134 ± 0.016	11.68/8
0.7-8.0	6.42 ± 0.05	0.11 ± 0.05	0.78 ± 0.13	0.77 ± 0.06	0.61 ± 0.01	0.132 ± 0.016	10.27/8
0.9-8.0	4.96 ± 0.04	0.04 ± 0.04	0.77 ± 0.31	0.53 ± 0.05	0.61 ± 0.01	0.112 ± 0.017	8.94/8
1.1-8.0	3.50 ± 0.03	-0.09 ± 0.04	1.11 ± 0.10	0.35 ± 0.04	0.62 ± 0.01	0.117 ± 0.020	10.95/8
1.3-8.0	2.42 ± 0.02	0.06 ± 0.03	0.63 ± 0.14	-0.22 ± 0.03	0.37 ± 0.02	0.108 ± 0.024	10.19/8
1.5-8.0	1.74 ± 0.02	-0.04 ± 0.03	0.19 ± 0.19	-0.14 ± 0.03	0.39 ± 0.02	0.093 ± 0.028	8.00/8
1.7-8.0	1.30 ± 0.02	0.03 ± 0.02	0.76 ± 0.19	-0.11 ± 0.02	0.38 ± 0.02	0.099 ± 0.030	7.62/8
2.0-8.0	0.91 ± 0.01	0.04 ± 0.02	0.79 ± 0.11	-0.06 ± 0.01	0.38 ± 0.03	0.099 ± 0.036	8.14/8

[1] We fit the X-ray modulation profiles with a model consisting of two Fourier components. The mathematical form of the model is shown below:

$$I = A + BSin2\pi(\phi - \phi_0) + CSin4\pi(\phi - \phi_1)$$

where, A is the mean countrate while B and C are the amplitudes of the fundamental and the first harmonics, respectively.

[2] This parameter is the fractional modulation amplitude and gives a quantitative measure of the amount of variation in the pulse profile. This is defined as follows:

$$f_{amplitude} = \frac{I_{max} - I_{min}}{I_{max} + I_{min}}$$

Table 2: Summary of the energy spectral modeling of NGC 5408 X-1. Best-fitting parameters for the *phabs*(diskpn+pow)* model are shown.

	phabs(diskpn+pow)*[†]						
Dataset	n_H^a	$N_{disk}^b(\times10^{-2})$	Γ^c	$N_{pow}^d(\times10^{-4})$	Flux[e] $_{0.6-8.0keV}$	Flux[f] $_{Disk}$	χ^2/dof
Non-Dip Pre-Transition spectrum	$0.297^{+0.022}_{-0.022}$	$1.57^{+0.22}_{-0.27}$	$2.96^{+0.07}_{-0.07}$	$7.69^{+0.49}_{-0.48}$	$3.68^{+0.21}_{-0.23}\times10^{-12}$	$1.69^{+0.29}_{-0.33}\times10^{-12}$	233.03/179
Non-Dip Post-Transition spectrum	$0.435^{+0.036}_{-0.040}$	$4.27^{+0.83}_{-0.86}$	$2.97^{+0.17}_{-0.15}$	$8.64^{+1.42}_{-1.19}$	$6.71^{+0.70}_{-0.77}\times10^{-12}$	$4.35^{+0.89}_{-0.77}\times10^{-12}$	111.95/87
Average Dip spectrum	$0.313^{+0.152}_{-0.175}$	$0.45^{+0.54}_{-0.42}$	$2.92^{+0.61}_{-0.53}$	$1.78^{+1.05}_{-0.70}$	$0.96^{+0.62}_{-0.48}\times10^{-12}$	$0.51^{+0.82}_{-0.82}\times10^{-12}$	17.02/17

[a]

Total column density of hydrogen along the line of sight including the Galactic extinction (in units of 10^{22}cm^{-2}). We used the *phabs* model in XSPEC. [b] The normalization of the disk component. We used the *diskpn* model in XSPEC. The inner radius of the disk was fixed at $6GM/c^2$. The disk temperature was fixed at 0.149 keV to avoid parameter degeneracy (see text). [c] The photon index of the power law. [d] The normalization of the power law component. We used *pow* model in XSPEC. [e] The total unabsorbed X-ray flux (in units of ergs cm^{-2} s^{-1}) in the energy range of 0.6-8.0 keV. [f] The disk contribution to the total X-ray flux (in units of ergs cm^{-2} s^{-1}) in the energy range of 0.6-8.0 keV.